Hybrid Fault Diagnosis and Isolation for Component and Sensor of APU in a Distributed Control System

LU Feng[1], *YIN Zihan*[1], *ZHOU Xin*[1*], *ZHANG Yufei*[2], *WANG Qin*[2], *HUANG Jinquan*[1]

1. Jiangsu Province Key Laboratory of Aerospace Power Systems, Nanjing University of Aeronautics and Astronautics, Nanjing 210016, P.R. China;

2. Aviation Motor Control System Institute, Aviation Industry Corporation of China, Wuxi 214063, P.R. China

(Received 9 December 2021; revised 22 April 2022; accepted 9 May 2022)

Abstract: This paper addresses the gas path component and sensor fault diagnosis and isolation (FDI) for the auxiliary power unit (APU). A nonlinear dynamic model and a distributed state estimator are combined for the distributed control system. The distributed extended Kalman filter (DEKF) is served as a state estimator, which is utilized to estimate the gas path components' flow capacity. The DEKF includes one main filter and five sub-filter groups related to five sensors of APU and each sub-filter yields local state flow capacity. The main filter collects and fuses the local state information, and then the state estimations are feedback to the sub-filters. The packet loss model is introduced in the DEKF algorithm in the APU distributed control architecture. FDI strategy with a performance index named weight sum of squared residuals (WSSR) is designed and used to identify the APU sensor fault by removing one sub-filter each time. The very sensor fault occurs as its performance index WSSR is different from the remaining sub-filter combinations. And the estimated value of the soft redundancy replaces the fault sensor measurement to isolate the fault measurement. It is worth noting that the proposed approach serves for not only the sensor failure but also the hybrid fault issue of APU gas path components and sensors. The simulation and comparison are systematically carried out by using the APU test data, and the superiority of the proposed methodology is verified.

Key words: auxiliary power unit (APU); gas path fault; sensor fault diagnosis and isolation; packet loss model; Kalman filter

CLC number: V233.7 **Document code:** A **Article ID:** 1005-1120(2022)04-0467-15

0 Introduction

It is well known that the auxiliary power unit (APU), an important subsystem of the aircraft, is a miniature gas turbine engine that is self-contained and requires no external energy[1]. APU provides power, gas, and hydraulic energy for the aircraft during the flight and restarts the engine in the event of an in-flight shutdown[2]. The operating condition should be supervised in real-time, and it guarantees the APU reliability and stability[3]. Sensor measurements are the primary sources of APU status information, and the accuracy of measurements is critical for APU control, performance monitoring, and diagnostics. Due to the harsh working environments and variable operating conditions of the aircraft, the sensors are fault-prone parts[4]. Various failures of the APU control system result from inaccurate readings. Hard redundancy and soft redundancy are two primary ways to improve the sensor reliability of the APU control system. The additional devices are usually installed by hard redundancy, leading to a weight increase. Hence, this paper mainly focuses on soft redundancy. The estimated measurements from the mathematical model are drawn and re-

*Corresponding author, E-mail address: zhouxin_203@nuaa.edu.cn.

How to cite this article: LU Feng, YIN Zihan, ZHOU Xin, et al. Hybrid fault diagnosis and isolation for component and sensor of APU in a distributed control system[J]. Transactions of Nanjing University of Aeronautics and Astronautics, 2022, 39(4): 467-481.

http://dx.doi.org/10.16356/j.1005-1120.2022.04.008

placed with the fault sensor measurements in APU as the hard redundancy fails[5].

The Kalman filter (KF) is a widely used method to realize engine soft redundancy and it reduces the computational burden under the distributed control system. Significant advances in distributed filters research have been made since the early 1970s. The structure of distributed filters with multiprocessors has been proposed. Each computing unit related to the node sensor was used to process the information obtained at all nodes, and each node got the overall results[6]. Furthermore, the architecture of a global filter with multiple sub-filters was developed and sub-filters were independent of each other. That the global filter completes the fusion of local results reduces the communication burden between sub-filters[7]. To realize the diminution of the network communication burden, Ribeiro derived a recursive algorithm named sign of innovations-Kalman filter (SOI-KF) for distributed state estimation based on residual markers[8]. Safari et al. developed a novel sensor fusion method for multi-rate sensor network systems via a neural network approach to estimate state vectors[9]. Chen et al. proposed a finite time domain federated Kalman filter algorithm to reduce the computation burden of filter and improve the sensor fault tolerance of multi-sensor network systems[10]. In the situation of a bias fault, Qiu et al. designed an intelligent covariance online sequence extreme learning machine (COSELM) algorithm to tackle the signal reconfiguration problem of the sensor[2].

GAO proposed a distributed extended Kalman filter (DEKF) algorithm with one main filter and five sub-filters to estimate health parameters[11]. Each sub-filter was designed independently and computed in parallel[12-13]. The pre-obtained local results were transmitted to the main filter for information fusion to get a global posterior estimation. The main filter assigned information to the sub-filters and state estimation fed back to sub-filters based on the global estimation[14]. A packet loss model was introduced to reflect the random occurrence of packet loss in measurements transmission from local sensors to the main filter[11,15]. The likelihood of packet loss for each sensor was considered to be the same and constant at all times[11]. A state receiving matrix was constructed according to the measurement transmission conditions after the packet loss probability was set. An improved DEKF algorithm with a packet loss model was presented by taking the state receiving matrix into account.

The estimated value of the sensor was calculated by the DEKF algorithm, and a performance index named weight sum of squared residuals (WSSR) was used to identify the APU sensor fault[16-18]. The sensor was faulty as its WSSR was different from the remaining sub-filter combinations, and the estimated value of the sensor at a fault-free time was used to replace the fault value. Then, compared with the original WSSR values[19-21], all the WSSR values after isolation were less than the threshold, and the isolation was regarded as successful.

In this paper, due to the extreme sensor working environments such as high temperature, five sensors are measurable and employed to estimate two flow capacity coefficients that are not obtained directly. The measurements are rotation speed sensor, compressor outlet temperature sensor, compressor outlet pressure sensor, turbine outlet temperature sensor, and turbine outlet pressure sensor. While the two flow capacity coefficients are compressor flow coefficient and turbine flow coefficient. Different from the research mentioned above, the innovation of this paper lies in a new application of the DEKF algorithm with random packet loss on the APU. The DEKF algorithm estimates the air path flow capacity coefficients not only in normal conditions, but also in the situation of sensor failures. Single and dual sensor faults are considered in the estimation process as two typical failure modes. The simulation results show that the isolation module eliminates sensor faults in a timely and effective manner in both types of sensor failures and ensure that the estimation of flow capacity coefficients remains correct and unaffected from the faulty sensors.

The roadmap of this paper is as follows. In Section 1, the nonlinear dynamic model of APU is introduced. Two flow capacity coefficients are employed to characterize the gas path flow characteris-

tics of APU components and the structure of adaptive model with Kalman filter bank is introduced briefly. Section 2 presents the DEKF algorithm with a packet loss model. Sensor fault isolation logic in the situation of single sensor fault or dual sensor fault is introduced in Section 3. Structure of APU sensor fault detection and isolation system and workflow of fault isolation mechanism are presented. In Section 4, gas path fault, sensor fault and hybrid fault are simulated and discussed respectively to verify the feasibility of diagnosis and isolation. Finally, some conclusions are summarized in Section 5.

1 APU Model and Problem Setup

This paper focuses on a single-spool APU. Gas path components of the APU include inlet, compressor, combustor, turbine, and nozzle. The APU nonlinear dynamic model is written by TMATS and works in SIMULINK. And it is established on the basis of component level engine modeling theories. Firstly, the mathematical model of each component is built according to the characteristics of APU components and design point parameters. Then, the cooperative working equations of components are established based on the principles of power balance and rotor dynamics. Finally, the numerical value iteration algorithm is employed to solve the equations to obtain the parameters of each working section. The flight condition parameters of the established model are flight altitude H, Mach number Ma, and inlet temperature. The nonlinear dynamic model of the APU is presented as

$$\begin{cases} \boldsymbol{x}_{k+1}=f(\boldsymbol{x}_k,u_k)+\boldsymbol{w}_k \\ \boldsymbol{y}_k=g(\boldsymbol{x}_k,u_k)+\boldsymbol{v}_k \end{cases} \tag{1}$$

where k is the time index, and $\boldsymbol{x}_k$, u_k and $\boldsymbol{y}_k$ denote the state variables, input variables and sensor measurements at time k, respectively. The model input variable is combustion chamber fuel flow W_f. The state variables of the model include rotation speed n and flow capacity coefficients $\boldsymbol{h}$, $\boldsymbol{x}=[n,\boldsymbol{h}^{\mathrm{T}}]^{\mathrm{T}}$. $\boldsymbol{w}_k$ and $\boldsymbol{v}_k$ represent uncorrelated system noise and measurement noise respectively, meeting $\boldsymbol{w}_k\sim N(0,\boldsymbol{Q}^2)$, $\boldsymbol{v}_k\sim N(0,\boldsymbol{R}^2)$. Here $\boldsymbol{Q}$ and $\boldsymbol{R}$ are the noise covariance matrices of system noise and measurement noise, respectively. $f(\cdot)$ and $g(\cdot)$ are the state transition function and measurement function of the APU model, respectively. The output parameters include rotation speed n, compressor outlet temperature T_3, compressor outlet pressure P_3, turbine outlet temperature T_5 and turbine outlet pressure P_5.

Due to the limitation of the number of sensors and the internal structure of the established APU model, only the flow capacity coefficients are chosen to be estimated accurately. Two flow capacity coefficients characterize the gas path flow characteristics of APU components completely. Considering that the performance of gas path components will inevitably change during the actual operation of the APU, the flow capacity coefficients are introduced to characterize the flow capacity degradation caused by individual performance differences or operation time of the APU. The flow capacity coefficients of gas path components $\boldsymbol{h}$ are presented as $\boldsymbol{h}=[CW,TW]^{\mathrm{T}}$, which are defined as

$$CW=\frac{A_1}{A_1^*},\quad TW=\frac{A_2}{A_2^*} \tag{2}$$

where A is the actual flow of components and A^* the ideal value. The subscript 1 represents the compressor and subscript 2 the turbine. The parameters CW and TW are the flow capacity coefficients of compressor and turbine, respectively. By expanding the state variables $\boldsymbol{x}=[n,\boldsymbol{h}^{\mathrm{T}}]^{\mathrm{T}}$, the corresponding APU model in Eq.(1) is the expanded model.

APU may have gas path faults or sensor faults, or both. It is very important to judge whether the changes in sensor measurements are caused by gas path faults or sensor faults. Firstly, in the situation of gas path faults, this paper will verify the estimation accuracy of flow capacity coefficients without adding sensor faults. Then, gas path faults and sensor faults are added at the same time. All sensor faults are eliminated as long as the threshold is set appropriately, and the injected gas path fault is still estimated correctly. The centralized Kalman filter (CKF) processes all the sensor measurements in one Kalman filter, so the sensor fault tolerance is poor. When a sensor fails and outputs error measurements, the CKF needs to be terminated and redesigned to select the correct sensors, so the continu-

ous operation of the filtering algorithm is difficult. In comparison, the sensor fault tolerance of DEKF is higher. When a sensor fails, the DEKF only needs to take measures to isolate the faulty sub-filter, and the filtering algorithm is carried out continuously. Fig.1 shows the structure of an adaptive model with Kalman filter bank, where $\boldsymbol{y}$ are the sensor measurements, $g(\boldsymbol{x}, u)$ outputs of APU model, and $\Delta\boldsymbol{y}$ the difference of y and $g(\boldsymbol{x}, u)$.

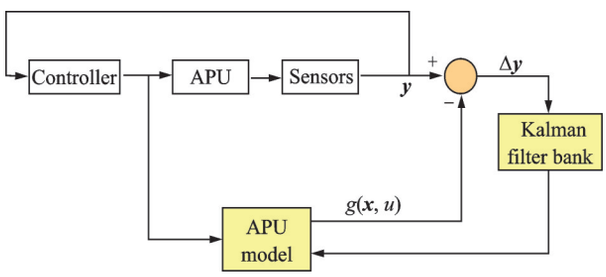

Fig.1 Adaptive model structure based on Kalman filter bank

Fig.1 presents an adaptive model with the Kalman filter bank which contains six Kalman filters and each one uses the DEKF algorithm. In every Kalman filter, each sub-filter only corresponds to one sensor, and this simplifies the data transmission and is not easy to make mistakes. The transmission structure is miniaturized and the weight of hardware equipment is reduced. A single sensor also minimizes the impact of noise interference. Compared with the traditional CKF, distributed filters adopt a parallel processing structure and share the computational burden of the main filter.

2 DEKF Algorithm with Packet Loss Model

2.1 DEKF algorithm

For a multi-sensors system such as the APU model, sensors are grouped to divide into different subsystems. Each sensor corresponds to a sub-filter, which is designed independently and calculated in parallel. The results obtained from sub-filters are transmitted to the main filter for information fusion and global posteriori estimation is obtained. The main filter will allocate information to sub-filters according to the global posteriori estimation and reset the sub-filters' state. Denote the total number of sub-filters as M, the calculation process of DEKF is written as follows.

(1) Posteriori estimation results $x_{0|0}$ and $P_{0|0}$ are initialized.

(2) Main filter information distribution is given by

$$\begin{cases} \boldsymbol{Q}^i = \boldsymbol{Q}/\beta_i \\ \boldsymbol{P}^i_{k|k} = \boldsymbol{P}_{k|k}/\beta_i \qquad \sum_{i=1}^{M}\beta_i = 1 \\ \boldsymbol{x}^i_{k|k} = \boldsymbol{x}_{k|k} \end{cases} \tag{3}$$

(3) Sub-filters calculate the local filtering results.

Time update

$$\begin{cases} \boldsymbol{x}^i_{k|(k-1)} = f(\boldsymbol{x}^i_{(k-1)|(k-1)}, u_{k-1}) \\ \boldsymbol{P}^i_{k|(k-1)} = \boldsymbol{A}\boldsymbol{P}^i_{(k-1)|(k-1)}\boldsymbol{A}^{\mathrm{T}} + \boldsymbol{Q}^i \end{cases} \tag{4}$$

Measurement update

$$\begin{cases} \boldsymbol{K}^i_k = \boldsymbol{P}^i_{k|(k-1)}\boldsymbol{C}^{i\mathrm{T}}(\boldsymbol{C}^i\boldsymbol{P}^i_{k|(k-1)}\boldsymbol{C}^{i\mathrm{T}} + \boldsymbol{R}^i)^{-1} \\ \boldsymbol{x}^i_{k|k} = \boldsymbol{x}^i_{k|(k-1)} + \boldsymbol{K}^i_k[\boldsymbol{y}^i_k - g(\boldsymbol{x}^i_{k|(k-1)}, u_{k-1})] \\ \boldsymbol{P}^i_{k|k} = (\boldsymbol{I} - \boldsymbol{K}^i_k\boldsymbol{C}^i)\boldsymbol{P}^i_{k|(k-1)} \end{cases} \tag{5}$$

The calculation process of Jacobian matrices $\boldsymbol{A}$ and $\boldsymbol{C}$ is as follows

$$\boldsymbol{A} = \frac{\partial f(\boldsymbol{x}_k, u_k)}{\partial \boldsymbol{x}_k}, \quad \boldsymbol{C} = \frac{\partial g(\boldsymbol{x}_k, u_k)}{\partial \boldsymbol{x}_k} \tag{6}$$

where i is the sub-filter number, $\boldsymbol{K}^i_k$, $\boldsymbol{C}^i$, $\boldsymbol{y}^i_k$, and $\boldsymbol{R}^i$ denote the Kalman gain, the Jacobian matrix, output variables and noise variance matrix related to the sub-filter i, respectively. The sub-filter is designed according to the above DEKF algorithm.

(4) Main filter information fusion is given by

$$\begin{cases} \boldsymbol{P}^{-1}_{k|k} = \sum_{i=1}^{M}(\boldsymbol{P}^i_{k|k})^{-1} \\ \boldsymbol{x}_{k|k} = \boldsymbol{P}_{k|k}\sum_{i=1}^{M}((\boldsymbol{P}^i_{k|k})^{-1}\boldsymbol{x}^i_{k|k}) \end{cases} \tag{7}$$

(5) Let $k = k+1$, and repeat from step (2) until the filtering process is completed.

Here $\boldsymbol{x}^i_{k|k}$, $\boldsymbol{P}^i_{k|k}$ and $\boldsymbol{Q}^i$ represent the local posteriori estimation, local posteriori variance matrix and noise variance matrix of the sub-filter i, respectively. β^i is the information distribution coefficient and meets the information conservation, which is usually taken as $\beta^i = 1/M$. In the APU model, the sensor number is five and the sensors are divided into

five groups ($M=5, \beta_i=0.2$).

2.2 Packet loss model

In the process of data transmission, the problem of flow capacity coefficients estimation in the situation of partial data loss is considered. For packet loss in data transmission, it is modeled by an independent identically distributed variable γ_k^c, which satisfies the 0-1 distribution. The probability distribution is written as

$$\begin{cases} Pr(\gamma_k^c=0)=p \\ Pr(\gamma_k^c=1)=1-p \end{cases} \tag{8}$$

where p is the probability of packet loss, c the APU sensor number, $\gamma_k^c=0$ means that the measurement $\boldsymbol{y}_k^c$ of sensor c at time k is not received by the filter, and $\gamma_k^c=1$ indicates that y_k^c is received on time at time k. Then, the measurements at time k are expressed as $\boldsymbol{y}_k=(\gamma_k^1\boldsymbol{y}_k^1, \gamma_k^2\boldsymbol{y}_k^2, \cdots, \gamma_k^N\boldsymbol{y}_k^N)^{\mathrm{T}}$, where N is the total number of sensors. The system measurement equation is expressed as

$$\boldsymbol{y}_k=\boldsymbol{\Lambda}_k[\,g(\boldsymbol{x}_k,u_k)+\boldsymbol{v}_k]=\tilde{g}(\boldsymbol{x}_k,u_k)+\tilde{\boldsymbol{v}}_k \tag{9}$$

where $\boldsymbol{\Lambda}_k=\mathrm{diag}(\gamma_k^1, \gamma_k^2, \cdots, \gamma_k^N)$ is the status receiving matrix, and γ_k^c the diagonal element of matrix $\boldsymbol{\Lambda}_k$. The variance matrix $\tilde{\boldsymbol{R}}_k=\mathrm{diag}(\tilde{r}_k^1, \tilde{r}_k^2, \cdots, \tilde{r}_k^N)$ of noise $\tilde{\boldsymbol{v}}_k$ has the following property

$$\tilde{\boldsymbol{r}}_k^c=\begin{cases} \boldsymbol{r}_c & \gamma_k^c=1 \\ \delta^2\boldsymbol{I} & \gamma_k^c=0 \end{cases} \tag{10}$$

when $\gamma_k^c=0$, γ_k^c is not received, $\delta\to\infty$. In DEKF algorithm, the nonlinear measurement equation of the system is rewritten as follows

$$\boldsymbol{y}_k=\tilde{g}(\boldsymbol{x}_k,u_k)+\tilde{\boldsymbol{v}}_k=\begin{bmatrix} \boldsymbol{\Lambda}_k^1 g^1(\boldsymbol{x}_k,u_k) \\ \vdots \\ \boldsymbol{\Lambda}_k^i g^i(\boldsymbol{x}_k,u_k) \\ \vdots \\ \boldsymbol{\Lambda}_k^M g^M(\boldsymbol{x}_k,u_k) \end{bmatrix}+\begin{bmatrix} \tilde{\boldsymbol{v}}_k^1 \\ \vdots \\ \tilde{\boldsymbol{v}}_k^i \\ \vdots \\ \tilde{\boldsymbol{v}}_k^M \end{bmatrix} \tag{11}$$

where $g^i(\boldsymbol{x}_k,u_k)$ is the nonlinear subsystem corresponding to the sub-filter i, and $\boldsymbol{\Lambda}_k^i$ and $\tilde{\boldsymbol{v}}_k^i$ are the subsystem state receiving matrix and the measured noise vector respectively. Eq.(5) is modified as

$$\begin{cases} \boldsymbol{K}_k^i=\boldsymbol{P}_{k|(k-1)}^i\boldsymbol{C}^{i\mathrm{T}}\boldsymbol{\Lambda}_k^{i\mathrm{T}}(\boldsymbol{\Lambda}_k^i\boldsymbol{C}^i\boldsymbol{P}_{k|(k-1)}^i\boldsymbol{C}^{i\mathrm{T}}\boldsymbol{\Lambda}_k^{i\mathrm{T}}+\tilde{\boldsymbol{R}}^i)^{-1} \\ \boldsymbol{x}_{k|k}^i=\boldsymbol{x}_{k|(k-1)}^i+\boldsymbol{K}_k^i\boldsymbol{\Lambda}_k^i[\,\boldsymbol{y}_k^i-g(\boldsymbol{x}_{k|(k-1)}^i,u_{k-1})\,] \\ \boldsymbol{P}_{k|k}^i=\boldsymbol{P}_{k|(k-1)}^i-\boldsymbol{K}_k^i\boldsymbol{\Lambda}_k^i\boldsymbol{C}^i\boldsymbol{P}_{k|(k-1)}^i \end{cases} \tag{12}$$

The structure of DEKF algorithm with packet loss model used in the APU model is shown in Fig.2.

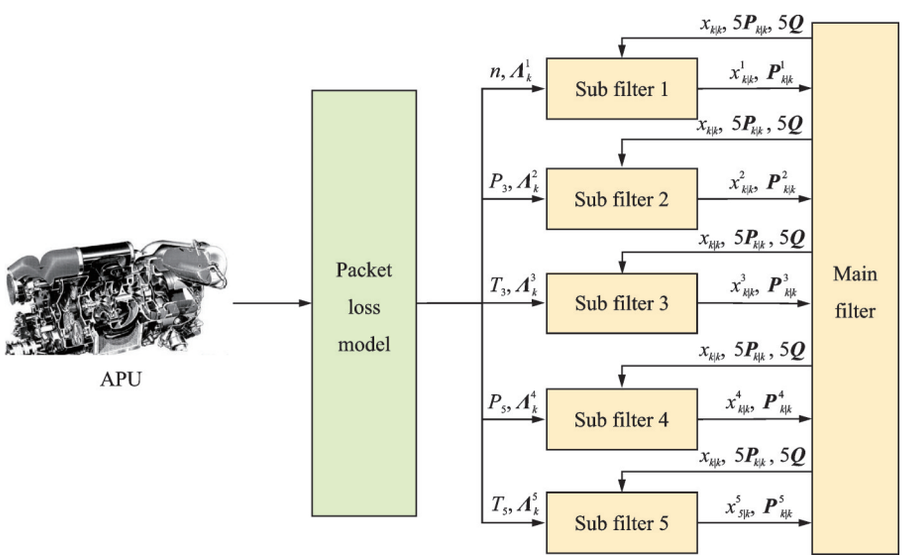

Fig.2 Structure diagram of DEKF algorithm with packet loss model

3 Sensor Fault Diagnosis and Isolation Logic

To alleviate the influence of faulty sensors, a sensor fault diagnosis and isolation system based on the Kalman filter bank is established, and the design principle is discussed. The APU sensor fault diagnosis and isolation system is mainly composed of an APU model, a measurements input module, a Kalman filter bank module, a fault diagnosis and isolation mechanism module, and a fault sensor reconfiguration module. The system is shown in Fig.3.

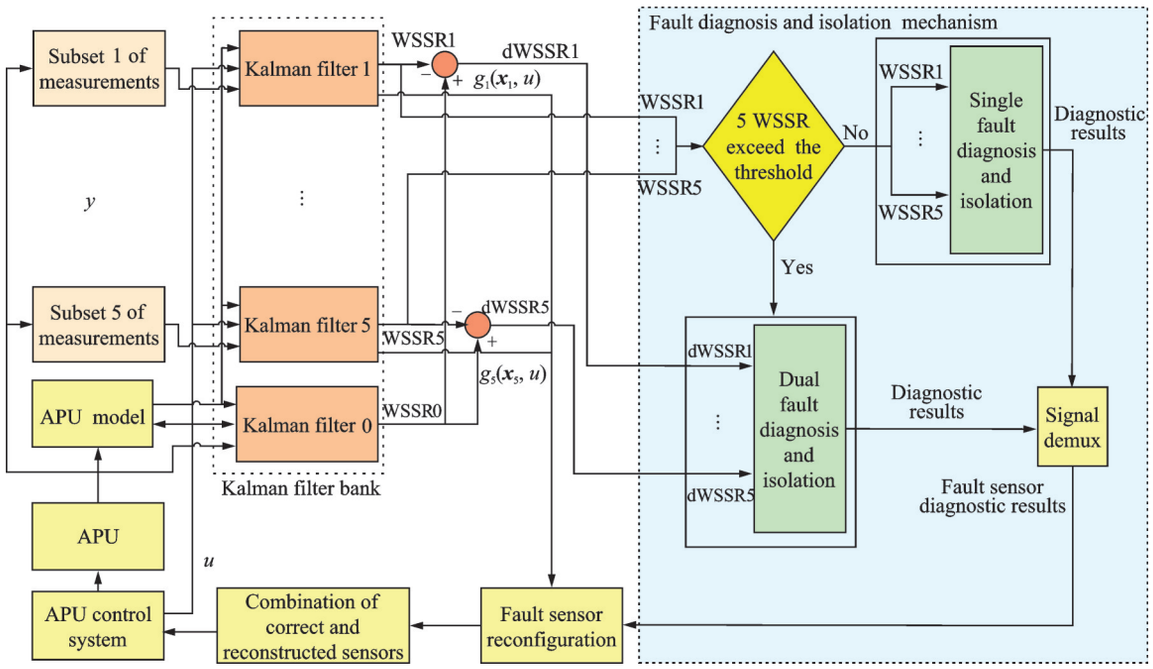

Fig.3 APU sensor fault diagnosis and isolation system

In Fig.3, y is the APU sensors measurements, u the input control value, $g(x, u)$ the outputs of APU model, $g_1(x_1, u)$ the estimated values of measurements in Kalman filter 1, and $g_5(x_5, u)$ the estimated values of measurements in Kalman filter 5. WSSR1 is the WSSR generated by Kalman filter 1, dWSSR1 is the dWSSR generated by Kalman filter 1, and others are the same. In the Kalman filter bank, the structure of Kalman filter 0 is the same as the one in Fig.2. Kalman filter 0 employs all 5 sensors to generate the WSSR which contains all the sensor fault information. Kalman filter 1 is the one without sub-filter 1, and its input sensor measurements named subset 1 of measurements include four sensors except for the rotation speed sensor. As a result, the WSSR generated by Kalman filter 1 contains sensor fault information of four sensors except for the rotation speed sensor. The same is true for other Kalman filters. The workflow of the fault diagnosis and isolation mechanism is shown in Fig.4.

When an APU sensor fails, the sensor measurement and the Kalman estimated value must not be consistent and these filter residuals containing the information of sensor fault will also change. The filter residuals are normalized by the filter weight sum of squared residuals $\boldsymbol{e}^{i\mathrm{T}}(\boldsymbol{\Sigma}^i)^{-1}\boldsymbol{e}^i$, which are named as the fault indication signal WSSR. Here $\boldsymbol{\Sigma}^i = [\mathrm{diag}(\sigma^i)]^2$, σ^i is the standard deviation of the ith sensor subset, and $\boldsymbol{e}^i$ the difference between the sensor measurement and the estimated value.

Since the measurement noise of the sensor is Gaussian white noise with zero mean value, $\boldsymbol{e}^i$ has the same property as the measurement noise. The fault isolation principle is that each Kalman filter is used to monitor a specific sensor and is designed based on fault-tolerant technology. When a sensor fails, the Kalman filter monitoring this faulty sensor only uses the measurements of other fault-free sensors, and the corresponding WSSR remains small. On the other hand, the others are Kalman filters in which the used subsets of measurements contain faulty information, and the related WSSR will increase and eventually exceed the preset threshold. Therefore, the faulty sensor is detected by setting a reasonable threshold and analyzing WSSR.

As shown in Fig.4, different subsets of the measurements are used as the input to the related Kalman filter. The estimated values of the corresponding sensors and WSSR are obtained by the Kalman filter bank. Through the analysis of WSSR, the fault isolation mechanism makes a judgment. The measurement is directly sent to the APU

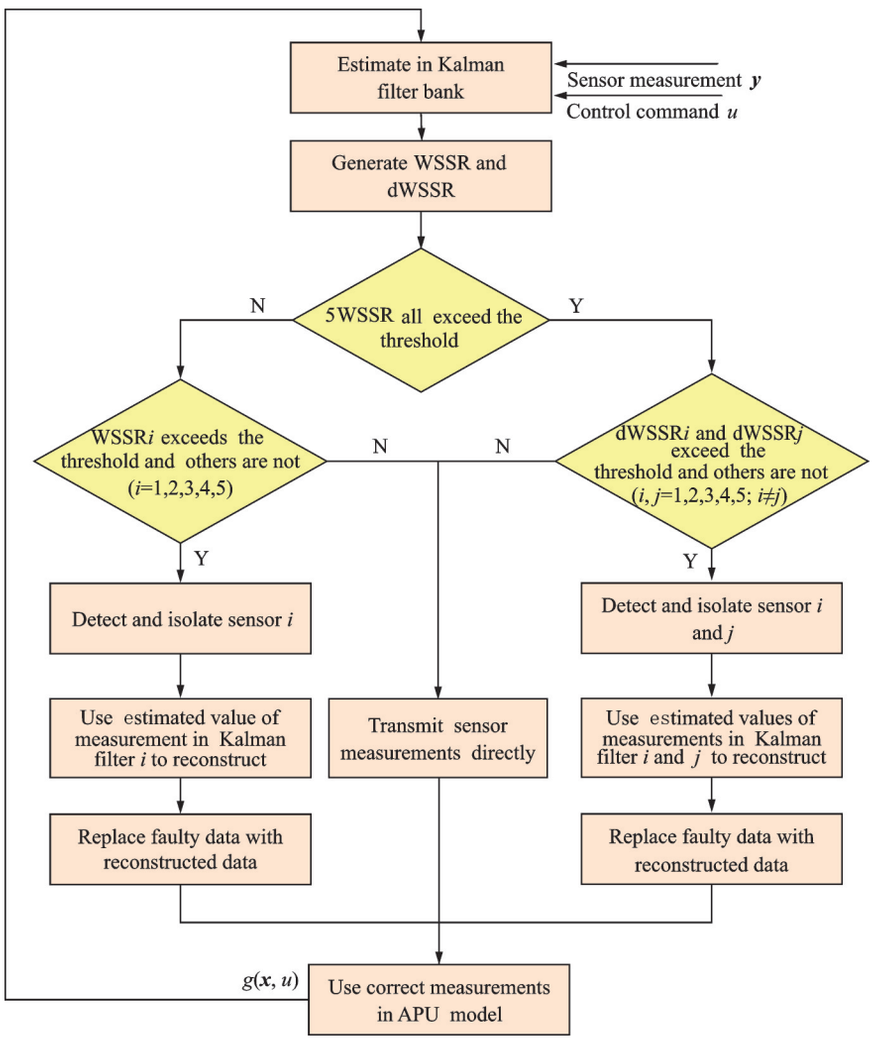

Fig.4 Workflow of APU fault diagnosis and isolation mechanism

control system while the sensor is fault-free, so the APU continues to operate safely and reliably. In the situation of sensor fault, the fault reconfiguration module is informed of the diagnosis result obtained by the fault isolation mechanism, and it reconstructs the corresponding fault sensor measurement.

A dual sensor fault refers to two sensors failing simultaneously. For the reason that more than one sensor has failed, the original fault diagnosis and isolation logic designed for a single sensor fault are no longer applicable. When a dual-sensor fault occurs, the five WSSR related to the five Kalman filters which sequentially remove one sensor will all exceed the threshold. It is easy to find that a dual-sensor fault has occurred by the analysis of WSSR, but it is impossible to tell which sensors have failed. For this reason, the diagnosis and isolation logic employed for dual-sensor fault is redesigned. Because the WSSR is the sum of residuals of the measured and estimated values of different sensors, it is cumulative naturally. The WSSR value of a dual-sensor fault should be higher than that of a single sensor fault, so an additional filter that does not remove any of the sensors is employed to record all the faulty sensor information by related WSSR. The WSSR output from this additional filter is named WSSR0. Eq.(13) is given by

$$\mathrm{dWSSR}i = \mathrm{WSSR0} - \mathrm{WSSR}i \tag{13}$$

where dWSSRi is the difference between WSSR0 and WSSRi.

That the corresponding dWSSRi will significantly exceed the threshold is the same in the situation that the ith sensor fails or a dual-sensor fault occurs, and the location of the faulty sensors is deter-

mined. When it is detected that all five WSSR are higher than the threshold, the saved APU sensor data is simulated again after the current simulation to isolate the dual-sensor fault. The schematic diagram of dual-sensor fault diagnosis is shown in Fig.3.

4 Simulation and Discussion

4.1 Gas path fault diagnosis

In this paper, n, P_3, T_3, P_5 and T_5 are selected as the measurements to be monitored by the APU. The appropriate noise whose corresponding covariance is $\boldsymbol{R}=[0.001\,5^2, 0.001\,5^2, 0.001\,5^2, 0.001\,5^2, 0.001\,5^2]$[2] is added into the model.

The degradation is simulated in 60 s. The sampling time of the examined APU is set to 0.015 s and the total number of sampling steps is 4 000. A packet loss model with the packet loss probability of 10% is employed to reflect the data packet loss phenomenon. At the design point ($Ma=0, H=0$ km), the APU starts from the nominal condition, and flow capacity coefficients magnitudes at this condition are 1. Two anomaly modes simulation of APU gas path are carried out as follows.

(1) Abrupt degradation mode of gas path: Flow capacity coefficients deviate from their normal value suddenly. In the APU model, the situation that two flow capacity coefficients shift from their nominal values is presented as follows: −2% on CW, +1% on TW[11], and the occurring time of 1 s.

(2) Gradual degradation mode of gas path: Two flow capacity coefficients synchronously and linearly move to their terminal magnitudes from their nominal values in 60 s at the design point as follows: −2% on CW, and +1% on TW[22].

After testing, the flow capacity coefficients of the APU model are estimated in the range of about 0.98 to 1.02 due to the limitation of APU model structure. The results of flow capacity coefficients estimation at two typical modes are shown in Figs.5 and 6, where the red and black lines represent the true and estimated values, respectively.

From Figs.5 and 6, the gas path performance degradation is quickly tracked and accurately estimated at two typical modes in 60 s, and the DEKF combined with a packet loss model is tested to be effective in the case of abrupt or gradual degradation.

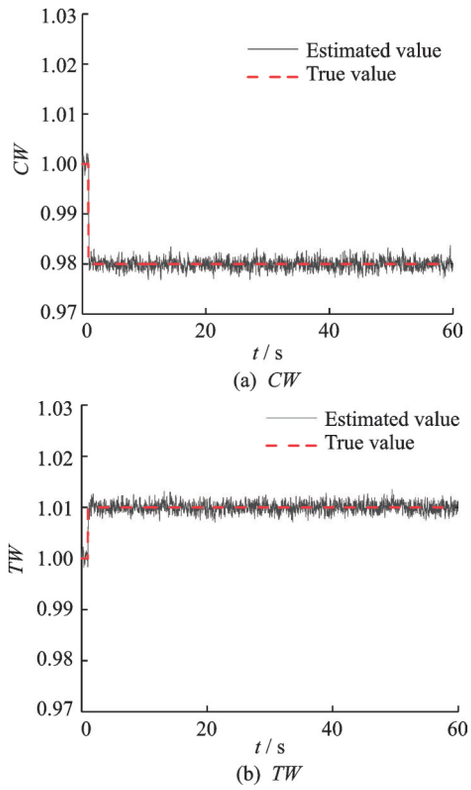

Fig.5 Abrupt degradation simulation of gas path components

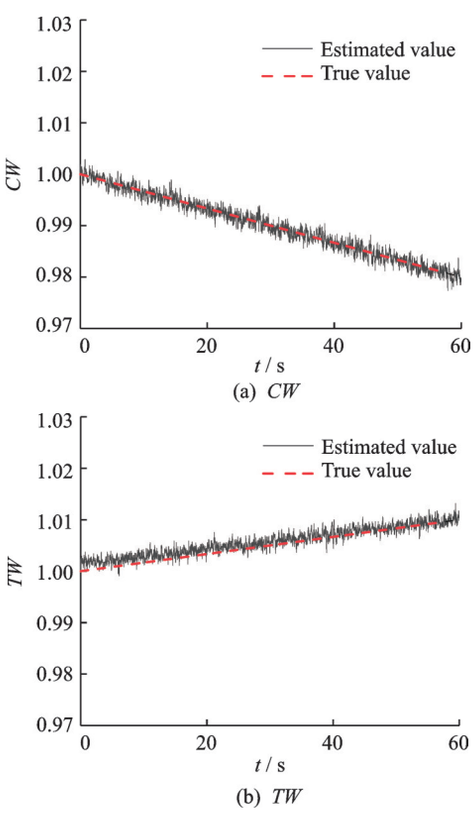

Fig.6 Gradual degradation simulation of gas path components

4.2 Sensor fault diagnosis

4.2.1 Single sensor fault diagnosis

The total simulation time is 60 s. It is assumed that n (Sensor 1) fails from 2.02 s to 4.02 s, P_3 (Sensor 2) from 12.02 s to 14.02 s and from 17 s to 17.07 s, T_3 (Sensor 3) from 24.02 s to 26.02 s, P_5 (Sensor 4) from 36.02 s to 38.02 s, and T_5 (Sensor 5) from 48.02 s to 50.02 s. The sensor failure types are intermittent bias failures, and the fault amplitude is 2%.

The reasonable threshold is the key to the whole sensor fault isolation system. On one hand, too large thresholds would lead to missed diagnosis and many faults are not detected. On the other hand, setting a too small threshold is easy to mistake the normal disturbance of some measurements as a fault. At the design point, the detection threshold is taken as 25 in the situation that sensors are no fault. The simulation results are shown in Fig.7.

It is worth noting that in Fig.7, except that the WSSR related to the fault sensor in the corresponding fault time still maintains a small value, the WSSR related to other sensors begin to increase in the above fault time and exceed the set detection threshold. Therefore, the fault isolation mechanism

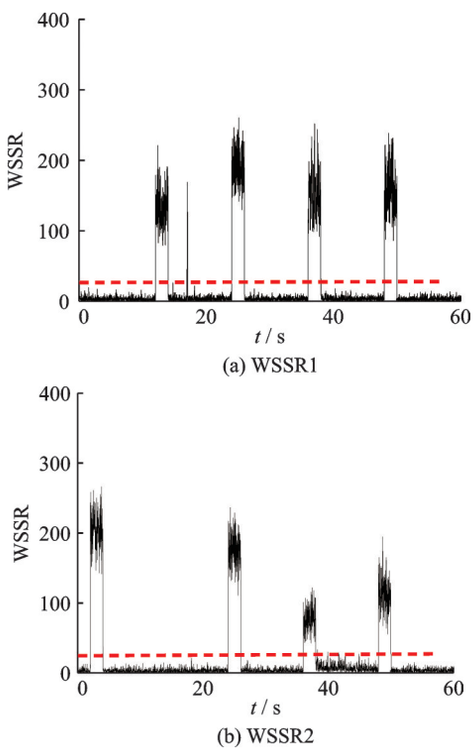

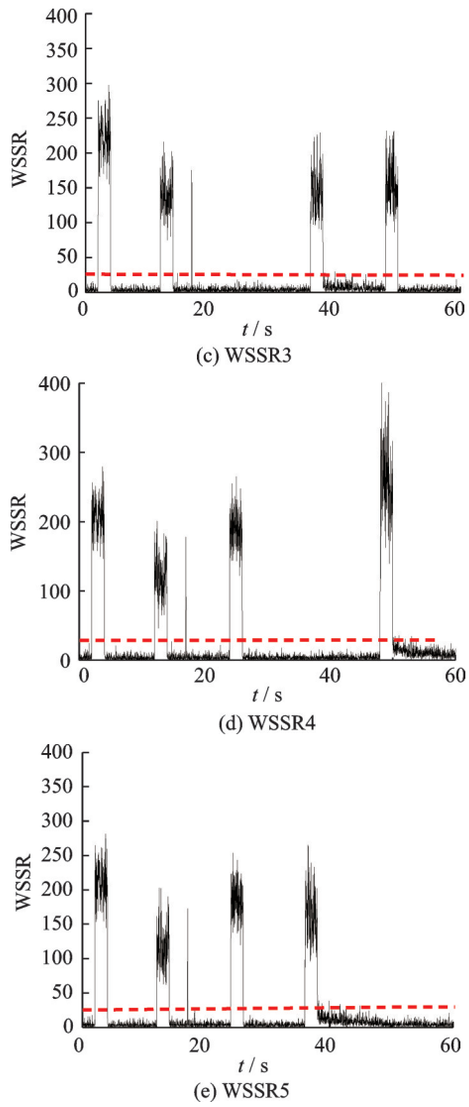

Fig.7 WSSR in the case of single sensor fault simulation

detects the occurrence of the bias fault and find which sensor has failed timely and accurately.

To avoid the usage of the wrong measurement, the sensor fault detection and isolation system combined with the Kalman filter bank replaces the faulty measurement with the estimated value of sensor measurement output from the Kalman filter which does not use the faulty sensor. Kalman filter 0 has all of five sensors and presents all the sensor fault information. WSSR0 related to Kalman filter 0 before and after isolation are shown in Fig.8.

From Fig. 8, WSSR0 is all smaller than the threshold in 60 s after isolation and the reconstructed value effectively avoids the Kalman filter bank from using the wrong measurement at the beginning of the fault.

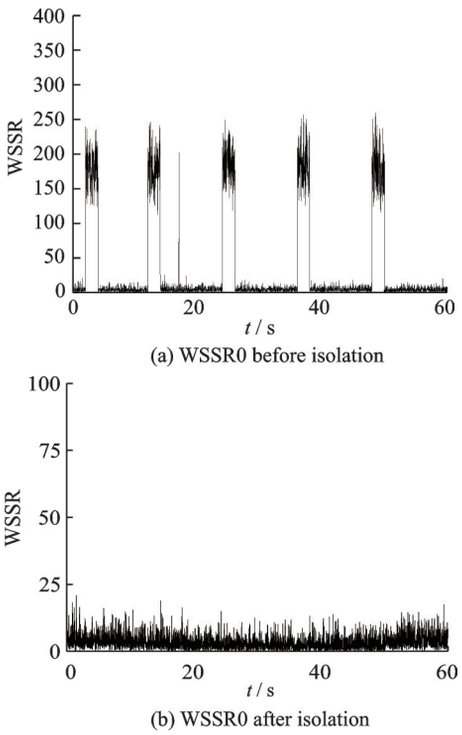

Fig.8 WSSR0 before and after isolation in the case of single sensor fault simulation

The fault amplitude has a great impact on the isolation accuracy. Generally speaking, the larger the amplitude is, the easier the fault is detected. The smaller the amplitude is, the easier the fault mixes with the measurement noise. In the situation that the amplitude is too small, likely the fault will not exceed the threshold at the beginning, so the fault isolation mechanism will still bring in the wrong value. Fig.9 shows the state of sensor fault isolation failure when each sensor tested is just at the lower limit of fault amplitude of isolation failure.

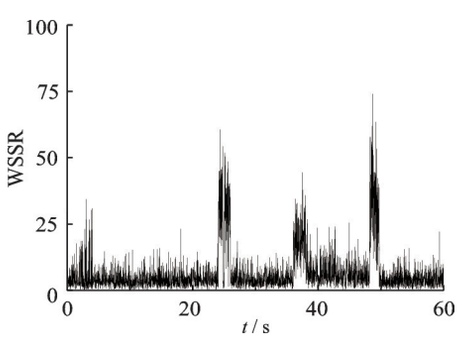

Fig.9 WSSR0 in the case of single sensor fault isolation failure

From Fig.9, except for P_3 sensor, the other sensors fail in isolation, but their lower limits of isolation failure are different. Table 1 shows the lower limit of isolation failure for each sensor and the isolation accuracy when the fault occurs.

Table 1 Amplitude lower limit and accuracy of each sensor isolation

Sensor	n	P_3	T_3	P_5	T_5
Amplitude/%	0.8	None	0.8	1.0	1.0
Accuracy/%	93.28	100	35.07	67.16	44.03

4.2.2 Dual sensor fault diagnosis

In the case of dual-sensor fault, the total simulation time is set to 60 s. n (Sensor 1) fails from 12.02 s to 50.02 s, P_3 (Sensor 2) from 19.02 s to 50.02 s, so a dual-sensor failure occurs from 19.02 s to 50.02 s. All fault types are bias faults and have an amplitude of 2%. The simulation results of the WSSR are shown in Fig.10.

From Fig.10, the five WSSR from WSSR1 to

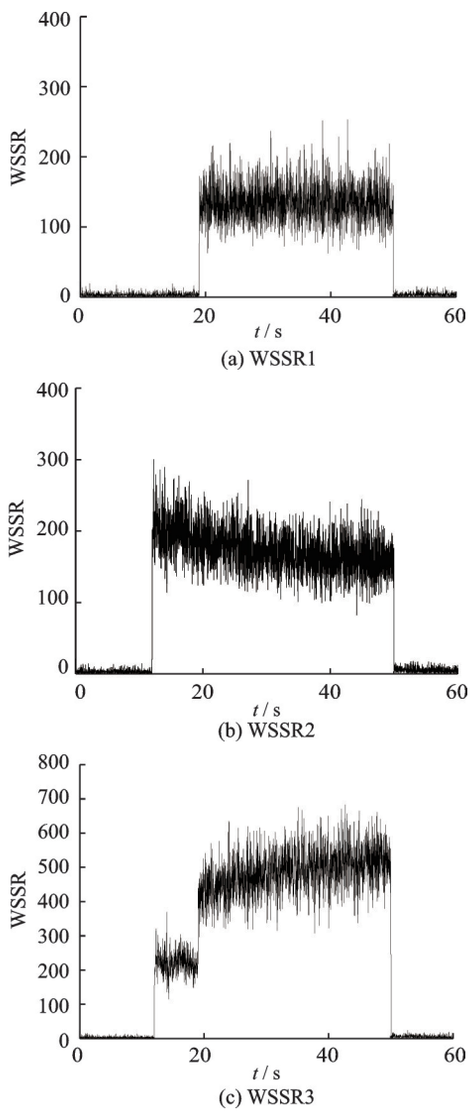

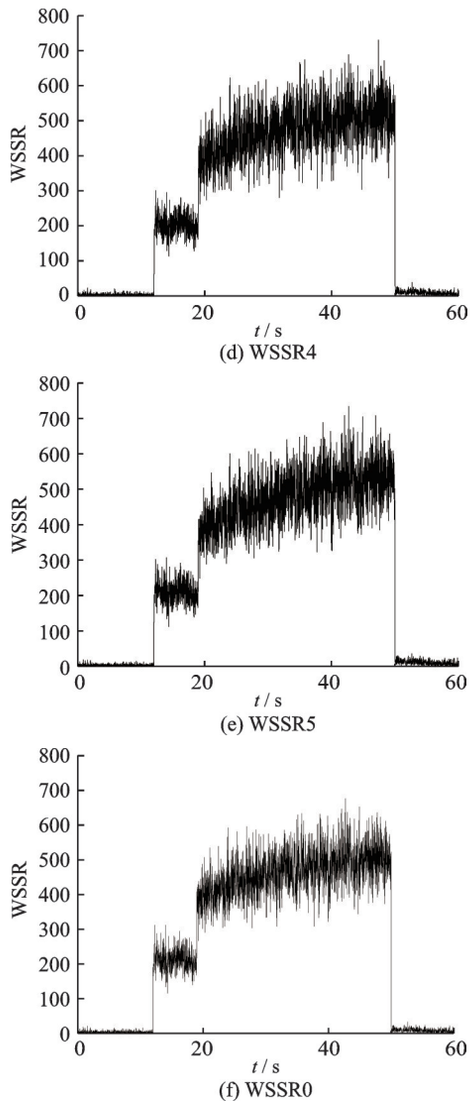

Fig.10 WSSR in the case of 2% bias faults of n and P_3 sensor simulation

WSSR5 all exceed the threshold value 25 from 19.02 s to 50.02 s when the dual sensor fault occurs, so it is impossible to tell which sensor is actually faulty. The WSSR0 from 19.02 s to 50.02 s is obviously larger than that of a single sensor fault occurring from 12.02 s to 19.02 s, so it is possible to use the cumulative nature of the WSSR. The WSSRi is subtracted from WSSR0 containing all fault information to obtain the corresponding dWSSRi. dWSSR simulation results are shown in Fig.11.

The threshold for dual-sensor fault is set to 100. Only the values of dWSSR1 and dWSSR2 exceed the threshold at the corresponding time of fault occurrence, and the rest of the dWSSR are less than the threshold. Both n and P_3 sensors fault con-

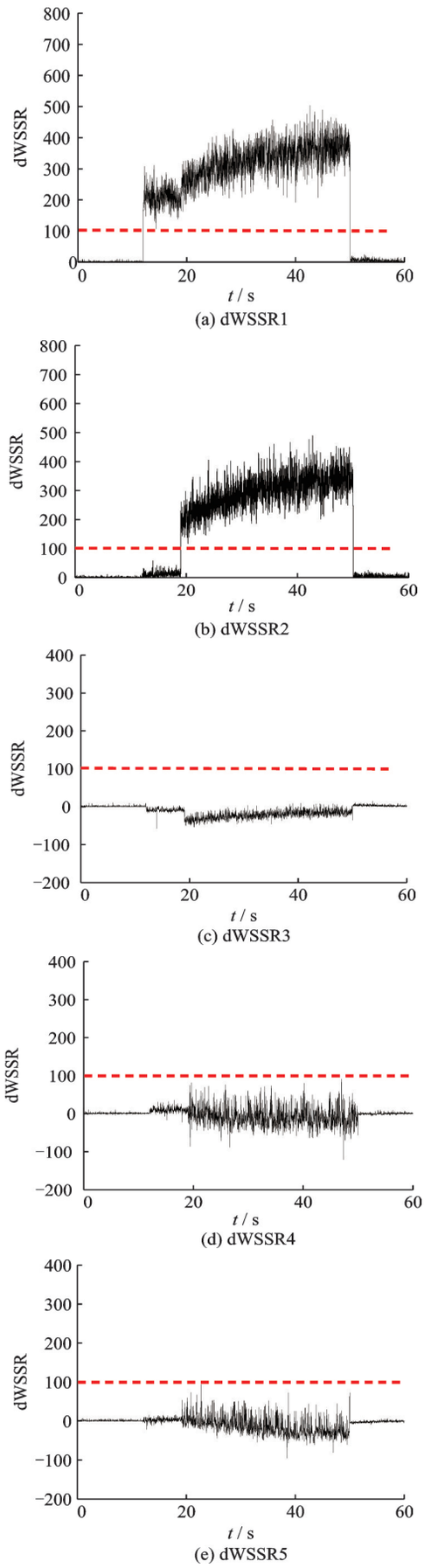

Fig.11 dWSSR in the case of 2% bias faults of n and P_3 sensor simulation

ditions are diagnosed from 19.02 s to 50.02 s after the onset of dual sensor fault. After isolation, the WSSR0 simulation result is shown in Fig.12.

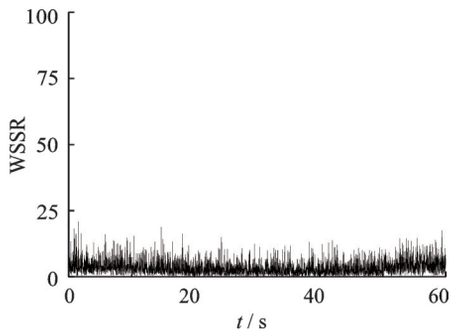

Fig.12 WSSR0 after isolation in the case of 2% bias faults of n and P_3 sensor simulation

It is easy to find that the reconstructed WSSR0 is less than the threshold in 60 s and the dual-sensor fault is successfully diagnosed and isolated.

4.3 Hybrid fault diagnosis

Sensor fault diagnosis simulation has been carried out to verify the feasibility of the Kalman filter bank on it. Then, sensor faults and gas path degradation are added simultaneously into the APU to more intuitively reflect the effect of sensor isolation, and the flow capacity coefficients tracking results are drawn before and after isolation.

4.3.1 Single sensor and component fault

In addition to the above sensor faults added in the single sensor fault situation, gas path abrupt degradation mode and gas path gradual degradation mode are employed to the APU respectively. The flow capacity coefficients estimation results of two anomaly modes before and after isolation are shown in Fig.13 and Fig.14, respectively.

From Figs. 13 and 14, during the period in which sensor fault occurs, the estimated values of flow capacity coefficients before isolation have abrupt changes, so the flow capacity coefficients are not estimated correctly. After isolation, the recon-

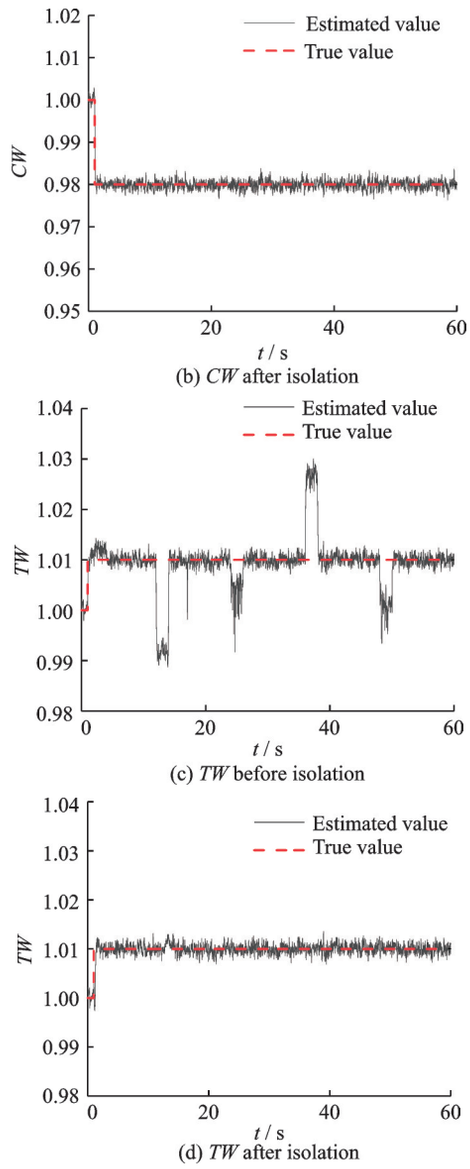

Fig.13 Flow capacity coefficient estimation in the case of single sensor fault with abrupt degradation of gas path

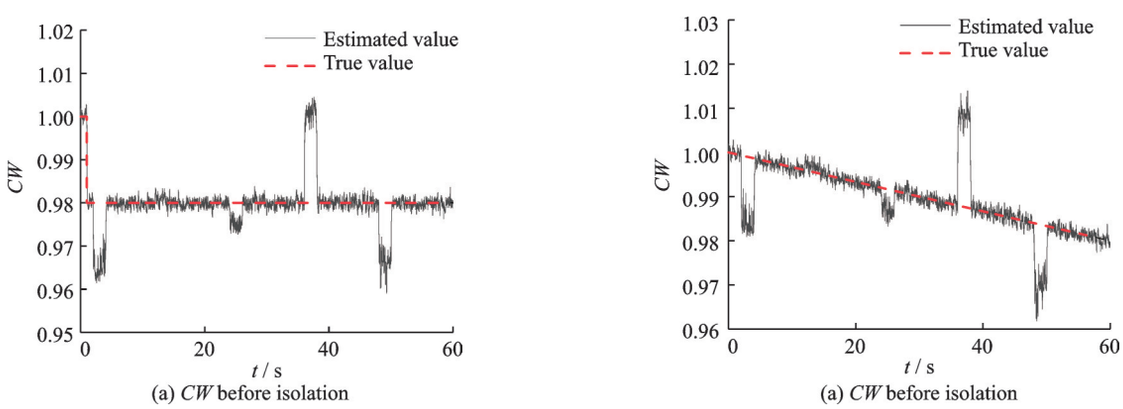

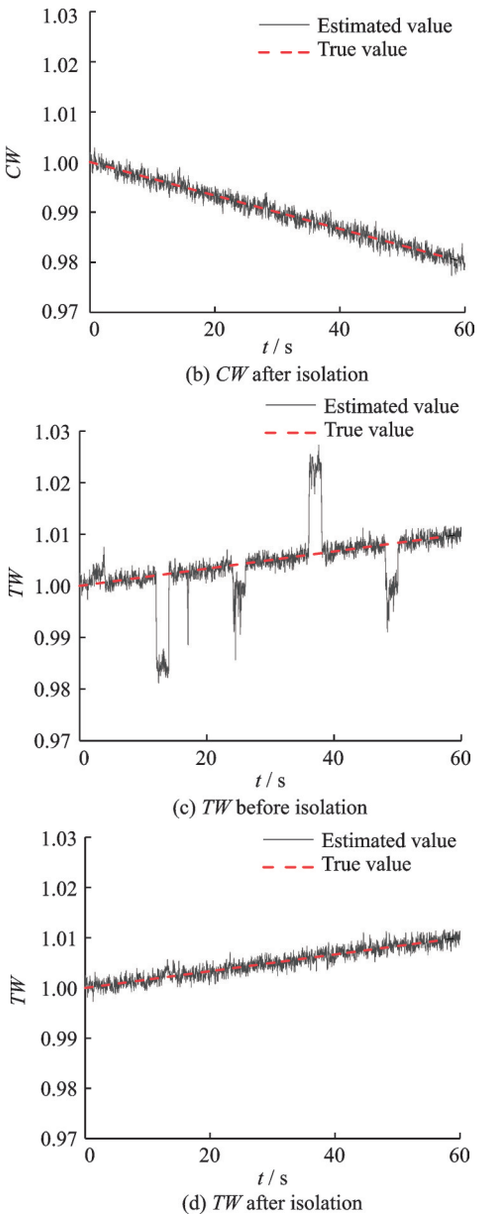

Fig.14 Flow capacity coefficient estimation in the case of single sensor fault with gradual degradation of gas path

structed sensor value replaces the wrong one, so the estimated values of flow capacity coefficients are the same as those without sensor fault. The isolation distinguishes gas path degradation from sensor fault, and the isolation effect is good.

4.3.2 Dual sensor and component fault

In addition to the above sensor faults added in a dual-sensor fault situation, the gradual degradation mode of gas path is employed to the APU. The flow capacity coefficients estimation results before and after isolation are shown in Fig.15.

In the case of dual sensor fault, the estimated

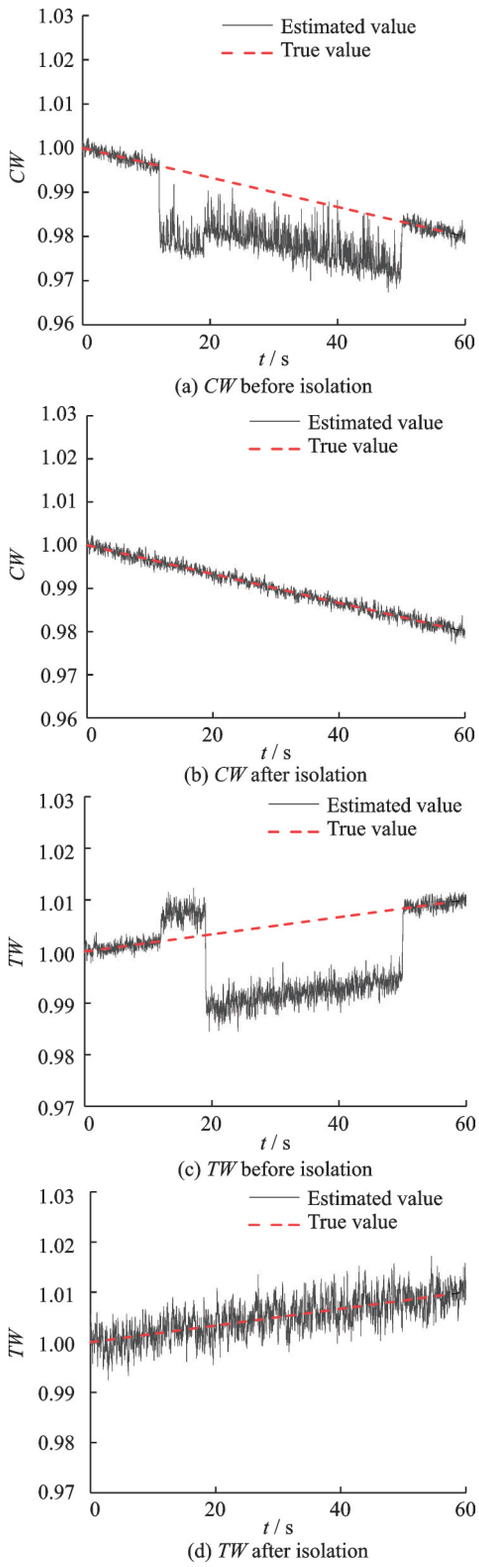

Fig.15 Flow capacity coefficient estimation in the case of dual sensor fault with gradual degradation of gas path

values of flow capacity coefficients before isolation have abrupt changes during the period in which the sensor fault occurs, so the flow capacity coefficients are not estimated correctly. After isolation, the flow

capacity coefficients satisfy the linear variation law.

5 Conclusions

This paper has proposed an application of the DEKF algorithm combined with a packet loss model on APU. The algorithm successfully estimates the flow capacity coefficients for gas path abrupt degradation and gas path gradual degradation in the situation of sensor faults.

In the steady condition, the fault detection and isolation of the five sensors are successfully realized under the distributed architecture by using the DEKF algorithm in single and dual-sensor fault conditions. When the gas path fault and sensor fault occur simultaneously, the sensor isolation module accurately distinguishes gas path degradation from sensor fault. The sensor faults are eliminated timely and effectively, so the estimation of flow capacity coefficients is still accurate and not affected by the faulty sensors.

References

[1] WANG Junqi, ZHAO Haigang, ZHANG Yuan. Flight test of steady and transient characteristics of APU[J]. Aeronautical Science and Technology, 2020, 31(9): 41-46.(in Chinese)

[2] QIU Xiaojie, ZHANG Yufei, WEN Binhe. Intelligent analytical redundancy method of control system sensors based on APU[J]. Journal of Aerospace Power, 2021, 36(6): 1177-1187.(in Chinese)

[3] WANG Qichen. Research on prediction of aircraft APU malfunction trend[D]. Tianjin: Civil Aviation University of China, 2020.(in Chinese)

[4] ZHANG Rong, HOU Lingfeng, ZHAO Xudong, et al. Method and apply of sensor signal reconfiguration for civil aero-engines[J]. Journal of Aerospace Power, 2016, 31(5): 1268-1274.(in Chinese)

[5] SUN Hao, GUO Yingqing, ZHAO Wanli. Information reconstruction algorithm of aero-engine sensors and actuators[J]. Journal of Beijing University of Aeronautics and Astronautics, 2020, 46(2): 331-339.(in Chinese)

[6] SIMON D. A comparison of filtering approaches for aircraft engine health estimation[J]. Aerospace Science and Technology, 2008,12(4): 276-284.

[7] LU F, GAO T Y Y, HUANG J Q, et al. A novel distributed extended Kalman filter for aircraft engine gas-path health estimation with sensor fusion uncertainty[J]. Aerospace Science and Technology, 2019 (84): 90-106.

[8] RIBEIRO A, GIANNAKIS G B, ROUMELIOTIS S I. SOI-KF: Distributed Kalman filtering with low-cost communications using the sign of innovations[J]. IEEE Transactions on Signal Processing, 2006, 54 (12): 4782-4795.

[9] SAFARI S, SHABANI F, SIMON D. Multirate multisensor data fusion for linear systems using Kalman filters and a neural network[J]. Aerospace Science and Technology, 2014, 39: 465-471.

[10] CHEN B, ZHANG W A, YU L. Distributed finite-horizon fusion Kalman filtering for bandwidth and energy constrained wireless sensor networks[J]. IEEE Transactions on Signal Processing, 2014, 62(4): 797-812.

[11] GAO Tianyangyi. Aeroengine gas path performance analysis method based on distributed filtering[D]. Nanjing: Nanjing University of Aeronautics and Astronautics, 2019.(in Chinese)

[12] JIANG Chunyu. Research on fusion filtering method for aeroengine gas path performance estimation[D]. Nanjing: Nanjing University of Aeronautics and Astronautics, 2018.(in Chinese)

[13] TIAN Di. Research on engine airborne adaptive modeling technology[D]. Nanjing: Nanjing University of Aeronautics and Astronautics, 2011.(in Chinese)

[14] LU F, GAO T Y Y, HUANG J Q, et al. Nonlinear Kalman filters for aircraft engine gas path health estimation with measurement uncertainty[J]. Aerospace Science and Technology, 2018 (76): 126-140.

[15] QIAN H M, QIU Z B, WU Y H. Robust extended Kalman filtering for nonlinear stochastic systems with random sensor delays, packet dropouts and correlated noises[J]. Aerospace Science and Technology, 2017 (66): 249-261.

[16] CHEN Yi. Research on sensors fault diagnostics of aeroengine control system[D]. Nanjing: Nanjing University of Aeronautics and Astronautics, 2007.(in Chinese)

[17] ZHAO Wenbo. Aero-engine sensor fault diagnosis and signal reconstruction[D]. Nanjing: Nanjing University of Aeronautics and Astronautics, 2011.(in Chinese)

[18] YUAN Y, LIU X F, DING S T, et al. Fault detection and location system for diagnosis of multiple faults in aeroengines[J]. IEEE Access, 2017(5): 17671-17677.

[19] ZHANG Peng. Aeroengine fault diagnostics based on

Kalman filter[D]. Nanjing: Nanjing University of Aeronautics and Astronautics, 2009.(in Chinese)

[20] XUE Wei, GUO Yingqing. Multiple sensors soft failure diagnosis for aircraft engine control system[J]. Computer Measurement & Control, 2007, 15(5): 585-586, 618.(in Chinese)

[21] ZHANG P, HUANG J Q. Aeroengine fault diagnosis using dual Kalman filtering technique[J]. Journal of Aerospace Power, 2008, 23(5): 952-956.

[22] WANG Zhe, GUO Yingqing, ZHAO Wanli. Measurement parameter selection of aeroengine health monitoring system based on Kalman filter[C]//Proceedings of the 40th Technical Exchange Conference and the 4th Joint Conference on Aerospace Power of the Third Professional Information Network of China Aerospace Industry-S11 Engine Control and Related Technologies. Kunming: [s.n.], 2019: 67-74.

Acknowledges This work was supported by the National Natural Science Foundation of China (No.91960110), the National Science and Technology Major Project (No.2017-I-0006-0007), and the Fundamental Research Funds for the Central Universities(NP2022418).

Authors Prof. **LU Feng** received the Ph.D. degree in aeronautical and astronautical science and technology from Nanjing University of Aeronautics and Astronautics, China, in 2009. His current research interests include aeroengine airborne modeling, aeroengine control, and aeroengine health management research.

Dr. **ZHOU Xin** received the Ph.D. degree in aeronautical and astronautical propulsion theory and engineering from Nanjing University of Aeronautics and Astronautics, China in 2021. Her current research interests include aeroengine modeling and intelligent control.

Author contributions Prof. **LU Feng** designed the research and contributed to the discussion and revision of manuscript. Mr. **YIN Zihan** conducted the simulation and wrote the manuscript. Dr. **ZHOU Xin** contributed to the discussion and revison of the manuscript. Dr. **ZHANG Yufei** provided the model and data for analysis. Dr. **WANG Qin** contributed to the background of the study. Prof. **HUANG Jinquan** contributed to the background of the study. All authors commented on the manuscript draft and approved the submission.

Competing interests The authors declare no competing interests.

(Production Editor: WANG Jing)

分布式控制系统下APU部件和传感器的混合故障诊断与隔离

鲁 峰[1], 殷梓晗[1], 周 鑫[1], 张宇飞[2], 王 琴[2], 黄金泉[1]

(1.南京航空航天大学航空动力系统江苏省重点实验室,南京 210016,中国; 2.中国航空发动机集团有限公司控制系统研究所,无锡 214063,中国)

摘要:研究了分布式控制系统下辅助动力装置(Auxiliary power unit, APU)的气路部件和传感器的故障诊断与隔离(Fault diagnosis and isolation, FDI),并在分布式控制系统中将非线性动态模型和分布式状态估计器结合起来进行了研究。分布式扩展卡尔曼滤波器(Distributed extended Kalman filter, DEKF)起到状态估计器的作用,用于估计气路部件的流动能力。DEKF拥有一个主滤波器和5组与APU的5个传感器一一对应的子滤波器,每个子滤波器产生局部状态的流动能力估计。主滤波器收集并融合局部状态信息,然后将状态估计反馈给子滤波器。在APU分布式控制结构的DEKF算法中引入了丢包模型。设计了具有残差加权平方和(Weight sum of squared residuals, WSSR)性能指标的FDI策略,并通过一次移除一个子滤波器来识别APU传感器故障。当前子滤波器的性能指标WSSR不同于剩余的子滤波器组合时,说明发生了传感器故障,并且解析余度的估计值会取代故障传感器的测量值。值得注意的是,该方法不仅适用于传感器故障,而且可以解决APU气路部件和传感器之间的混合故障问题。利用APU测试数据进行了系统性的仿真和比较,验证了该方法的优越性。

关键词:辅助动力装置;气路故障;传感器故障诊断与隔离;丢包模型;卡尔曼滤波器